Optical manipulation of the negative silicon-vacancy center in diamond

Michael Hanks,[1,2,*] William J. Munro,[3,2] and Kae Nemoto[2,1]

[1]*Department of Informatics, School of Multidisciplinary Sciences, Sokendai (Graduate University for Advanced Studies), 2-1-2 Hitotsubashi, Chiyoda-ku, Tokyo 101-8430, Japan*

[2]*National Institute of Informatics, 2-1-2 Hitotsubashi, Chiyoda-ku, Tokyo 101-8430, Japan*

[3]*NTT Basic Research Laboratories and NTT Research Center for Theoretical Quantum Physics, NTT Corporation, 3-1 Morinosato-Wakamiya, Atsugi, Kanagawa 243-0198, Japan*

(Received 31 July 2019; accepted 24 July 2020; published 24 August 2020)

The silicon-vacancy center in diamond has recently attracted significant attention as a candidate for quantum information processing as it overcomes many of the optical issues present in the nitrogen-vacancy center. Historically it has been hampered by short dephasing times; however the recent development of high-purity samples at low temperatures resolves this issue. Hence it is timely to explore whether silicon-vacancy centers are useful for quantum tasks beyond single-photon sources. Here we investigate the potential of the silicon-vacancy center to realize two important operations required for quantum information processing: high-efficiency projective measurement and efficient single-qubit rotations. Due to its similar nature, the germanium-vacancy center is discussed as a point of comparison.

DOI: 10.1103/PhysRevA.102.022616

I. INTRODUCTION

Substantial improvements in the speed and size of modern computers since the invention of the transistor over seventy years ago has changed almost every aspect of our lives. Landmark discoveries in quantum information science [1–3] promise advantages based on the principles of quantum physics that cannot be achieved with classical machines alone. The rapid advance in quantum science and technology has led to the exploration of many physical systems including quantum dots [4], dopants and crystal defects [5,6], trapped ions [7], and superconducting circuits [8,9] as candidate systems for quantum computation [10,11], communication [12,13], and metrological [14,15] tasks. Further, remarkable control in these systems [16–19] as well as mechanisms for protecting such systems from decoherence [20–22] have allowed many pioneering demonstrations to be performed [23,24]. No physical system however has all necessary attributes for the wide range of quantum tasks one is likely to require and so new physical systems need to be investigated.

One new and promising candidate system for quantum tasks is the negatively charged silicon-vacancy center defect in diamond (SiV^-). This proposes both an electron and nuclear spin as well as optical interface. As such it is suitable for quite a diverse range of quantum tasks [25]. It has been seen by many as a successor to the optically problematic nitrogen-vacancy center [26]. SiV^- consists of a single silicon atom at the center of a split vacancy, in the space left by the removal of two adjacent carbon atoms in the diamond lattice. Sukachev *et al.* [27] have shown excellent coherence properties for this center, measuring a T_2 time of 13 ms with a T_1 time exceeding 1 s. The center also displays long-lifetime nuclear spin storage [28], along with a hyperfine interaction (10–100 ns [25]) between the electronic and nuclear spin states in the ^{29}Si isotope. Stabilization of the spin state of the silicon-vacancy center gives us a reason to reconsider the potential of this center for the encoding, processing, and measurement of quantum information [29]. The key question to answer is whether the silicon-vacancy center provides a path around NV^- optical issues [30–35].

We know that quantum computing requires preparation, single- and two-qubit gates, and measurement. Current approaches with the SiV^- center operate in a regime of small magnetic fields at low temperatures to preserve the center's coherence time. However, high-fidelity single- and two-qubit gates necessary for future scalable quantum information processing have proven elusive. Recently, Bhaskar *et al.* [36] and Becker *et al.* [37] have demonstrated high-fidelity single-qubit measurement and initialization, but these cannot be used in typical entanglement generation and further may actually interfere with the information encoded in the ^{29}Si nuclear spin. Next, π-pulse fidelities close to 99% for a direct transition were obtained in [27]. This came at the cost of making such a direct transition between qubit states strongly allowed and reducing the lifetime of the upper qubit state. The authors of [27] observed spin measurement fidelities of order 90%. Operational fidelities for coherent population transfer through weakly allowed transitions have been limited to approximately 90% [38]. It appears that some significant change in approach will be necessary to overcome these issues in the common field regimes, or a different operating regime altogether (such as the strong magnetic field regime) will need to be found.

Here we theoretically investigate the spin measurement fidelity, mediated by cavity reflection [39–44], and its

*hanks@nii.ac.jp

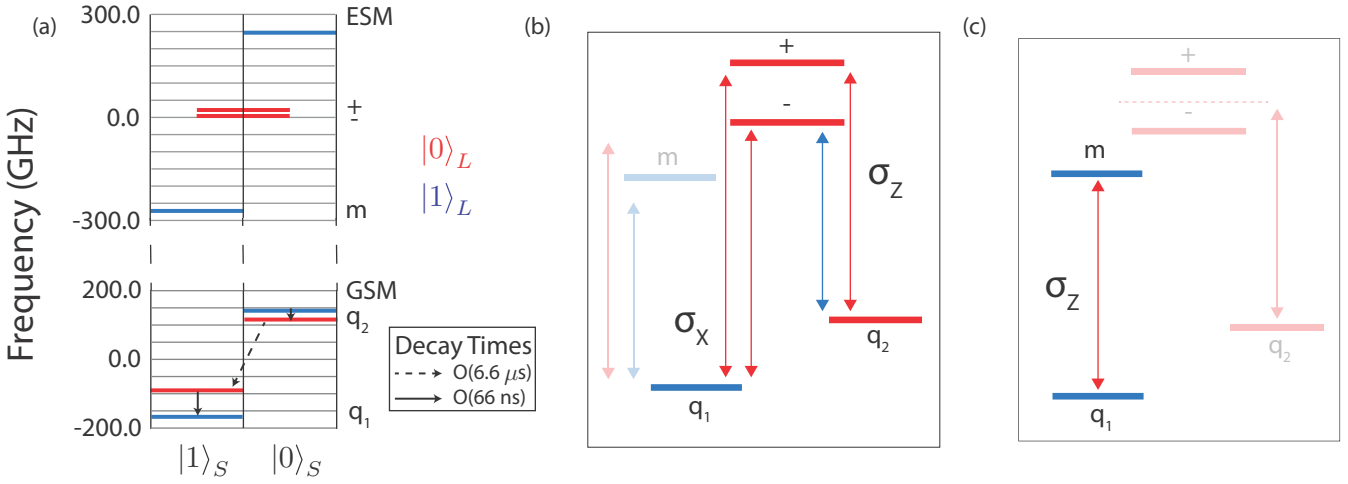

FIG. 1. (a) The energy level structure and ground-state relaxation rates of the negatively charged silicon-vacancy center ground and excited state manifolds (GSM and ESM) under the assumptions described in Sec. II, for a magnetic field with $B_Z = 9.179$ T and $B_X = 0.600$ T. Labels $(\pm, m, q_1, q_2)$ are added for those states significant to the main text. Decay rates are distinct from those of Sukachev *et al.* [27], because they are calculated for emissive decay (see Appendix A 3), whereas those cited values were measured for qubit states only in the lower branch of a regime qualitatively similar in structure to our zero-field case. All optical transitions preserve the spin state ($|\psi\rangle_S$, denoted by column), while Z-polarized optical transitions additionally preserve the orbital state ($|\psi\rangle_L$, denoted by color) and are coupled twice as strongly [25,47]. (b), (c) Transition diagrams for STIRAP population transfer as described in Sec. IV (b), and cavity-mediated spin measurement as described in Sec. III (c). $\sigma_{X/Z}$ denote the photon-polarization of driving fields. Arrows depict driven transitions, with red and blue arrows a factor $e^{i\pi}$ out of phase. Nearby undesirable transitions are also shown with partial transparency.

application to entanglement distribution in the strong-field regime. We further consider single-qubit manipulation using optical stimulated Raman adiabatic passage (STIRAP) [45]. Prior experimental work showing optical control [25,37,38,46] left open the question of the utility of a STIRAP pulse approach for high-fidelity operations on single spins. Our paper is organized as follows: In Sec. II we review the core properties of the silicon-vacancy center, while Secs. III and IV describe the cavity-mediated spin measurement and population transfer using STIRAP. Section V provides a point of comparison for measurement with the germanium-vacancy center, with Sec. VI summarizing our findings.

II. THE SILICON-VACANCY CENTER

The SiV^- center consists of four optically excited states (ES) and four lower-energy ground states (GS)—see Fig. 1—each associated with spin and orbital angular momentum components [25,47]. They are governed by Hamiltonians of the form

$$\hat{H} = \hbar\lambda \hat{S}_Z^{(o)} \hat{S}_Z^{(e)} + f\mu_B B_Z \hat{S}_Z^{(o)} + 2\mu_B \sum_i B_i \hat{S}_i^{(e)} + \hbar\epsilon_I \hat{S}_Z^{(o)2} + \hbar \sum_j \epsilon_j \hat{S}_j^{(o)}, \quad (1)$$

where $i \in \{X, Y, Z\}$ and $j \in \{X, Y\}$. Here $\hat{S}_{X/Y/Z}^{(o/e)}$ are spin-1/2 operators for the orbital (o) and spin (e) subsystems with the orbital operators containing an extra factor of 2 [47,48]. Next $\lambda = -2\pi \times 51.5$ GHz ($-2\pi \times 257$ GHz) denotes the spin-orbit coupling in the ground (excited) state manifold, GSM (ESM), while $f = 0.1$ reflects a dynamic Jahn-Teller suppression of the magnetic field on the orbital component [47]. Further, $\mu_B/\hbar = 2\pi \times 14.0\ \text{GHz}\,\text{T}^{-1}$ is the Bohr magneton, while $B_{X/Y/Z}$ are applied magnetic fields along each of the principal axes and $\epsilon_{I/X/Z}$ represent strain fields. The ES lifetimes are 1.8 ns [49].

At low temperatures ($T \leqslant 100$ mK) we assume decoherence is dominated by an Orbach process [48]. This process is limited by the excitation rate of the orbital component and subsequent relaxation from the upper branch of the ground states. This appears to occur in the orbital and spin components at a ratio of 100 : 1 based on relative T_1 and T_2 times of 1 s and 10 μs [27]. The zero-temperature orbital and spin relaxation rates from the upper branch are inferred from [48,50] to be 66 ns and 6.6 μs, respectively (see Appendix A 3 and Fig. 1).

Some parameter tuning is required if we want to use STIRAP to perform our single-qubit rotations. STIRAP requires coupling to the same intermediate excited state (or set of states), for which perturbative mixing is insufficient. Bringing the central excited states together to mix spin projections inverts the order of the two central ground states, reducing the qubit lifetime. We justify this by the 10 ns timescale of the operations, applying a magnetic field of $B_Z = 9.179$ T, $B_X = 0.600$ T. Further, the coherence time remains more than an order of magnitude larger than the expected hyperfine period. Finally, strain terms are set to zero and several optimistic assumptions are made (see Appendix A).

III. MEASUREMENT AND INITIALIZATION OF THE ELECTRONIC SPIN STATE

The most common means of measuring the spin state of the center has been resonance fluorescence [25,27,37,38,50–52]. This has been limited by population of the excited

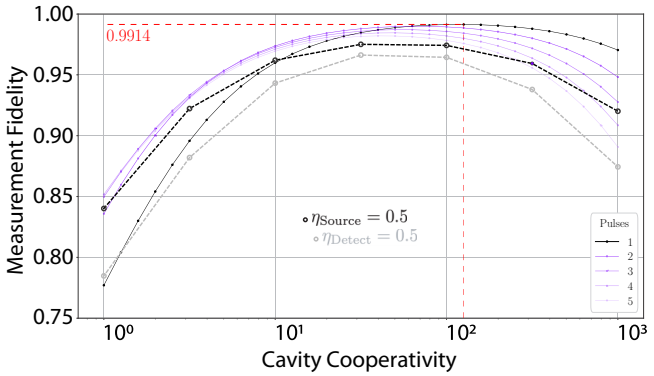

FIG. 2. Measurement fidelity as a function of the cooperativity and the number of single-photon pulses. Identified in red is the maximum observed fidelity, 0.9914. The dashed black (gray) curve shows the fidelity with a source (detection) efficiency of 0.5, maximized over the pulse number.

states, but strong Purcell enhancement using a two-photon process [42,53] with axially polarized transitions (having greater coupling and branching ratios [47]) provides a way to overcome this. Coherent states can be used to overcome loss and enhance coupling with the SiV^- center; however such techniques are not suitable for projective entanglement generation and so we will turn our attention to multiple single-photon pulses (which later could be relaxed to weak coherent pulses).

Our proposed measurement approach differs from the resonance fluorescence technique and instead relies on reflection from a coupled optical cavity. Here dependent on the SiV^- state, the scattering properties from the cavity change. A sequence of single photons then probes the state of the center using conditional reflection from the coupled cavity-center system. The scattering approach relies on two main assumptions: photon populations from pulses in succession do not interfere with one another and the bandwidth of the driving field is small. As such we have chosen a pulse width of 20 ns (after which $4.5 \times 10^{-3}\%$ of the population should remain) given the decay time is on the order of 1.8 ns. Further, the 20 ns width is also an order of magnitude greater than that at which the transmission or reflection probabilities diverge from the ideal case (∼3 ns; see Appendix B 2). Finally, the maximum number of probe pulses is limited to order 10 through the spin relaxation time.

In our cavity-assisted spin measurement, we want to perform two tasks: the first is to distinguish the different qubit basis states and the second is to project a superposition state into one of the basis states. As such let us consider the case where our SiV^- qubit is initially prepared in a 50/50 mixture. In Fig. 2 we show our estimated measurement fidelities against cooperativity, pulse number, and source and detection efficiency. We observe that maximum fidelities of order 99% are found for cavity cooperativities in the region 50–100, when ideal sources and detectors are assumed. This 99% maximum of course drops when we consider inefficiencies in our source and detectors. For a 50% detection (source) efficiency, the fidelity drops to order 96.6% (97.6%), increasing the number of single photons required from 1 to 7 (8). The chief limitation is temporary leakage to higher-energy ground states, resulting in significant dephasing and a non-negligible probability of spin-flip transitions. Our estimated spin decay time 6.6 μs is an extrapolation from a different field regime and so the possibility remains that lifetimes observed experimentally may exceed this estimate. An improvement of two orders of magnitude in the spin decay time would be required to obtain a measurement fidelity of 0.999 under our field configuration (see Appendix B 1). This would apply only to spin measurement and initialization and not to the projective entanglement generation, which degrades on the loss of entangled photons.

IV. POPULATION TRANSFER BETWEEN SPIN STATES

Single-qubit rotations with the SiV^- center have previously been demonstrated both directly between ground states [27] and indirectly using perturbative Raman transitions through the excited states [38]. Relying on perturbative spin-projection overlap leaves such processes vulnerable to decay, and the fidelity of optically mediated transitions has consequently been limited to around 90%. It remains an open question whether a STIRAP approach could be used to maintain population in the qubit subspace to avoid this. As described previously, the field configuration required for optical STIRAP alters the coherence properties of the ground states. Here we describe how this altered coherence interacts with constraints in the energy level structure, placing a limit on the fidelity of coherent population transfer. The spin state of the center does not change under optical excitation. Transfer between the qubit states must therefore involve at least two intermediary states. As shown in Fig. 1 the separation between these places a limit on the rate of the transfer of order $2\pi \times 10$ GHz. Further, a strong Stokes pulse may allow a transition to the lowest-energy excited state of the ESM (state "m" in Fig. 1), causing decoherence through rapid optical decay.

Now in our work here we use a Lindblad-based master equation approach to simulate coherent population transfer using the STIRAP process. We assume a 1.8 ns optical decay, 66 ns ground-state orbital decay, and 6.6 μs ground-state spin decay (see Sec. II and Appendix C). Further, the pulse time was chosen at 33 ns to limit ground-state spin relaxation to less than 1%. Following [54], we use Gaussian-shaped Stokes and pump pulses with the same profile (width and magnitude) that are separated by one standard deviation (33/8 ns). The frequencies and polarizations are chosen resonant with the target transitions. Our simulations show the best performance occurs with a maximum pulse amplitude at approximately 10% of the detuning between the intermediate states "±". The population dynamics for this driving amplitude are shown in Fig. 3. Here the degree of transfer is limited to order 97%, which is caused by a trade-off between the population transfer to the target ground state and to excited states resulting in rapid spontaneous decay. This can be observed in the comparable final populations of $|10\rangle_{LS}$, $|01\rangle_{LS}$, and $|11\rangle_{LS}$, and in the presence of slight oscillations in the transfer curve. As noted for spin measurement in the previous section, this trade-off limiting the performance of STIRAP population transfer could be improved to fidelities in the high nineties if the spin

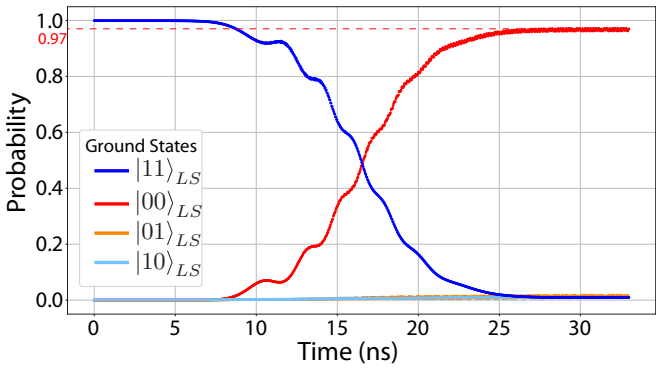

FIG. 3. State population probabilities versus STIRAP transfer time from qubit state q_1 [blue (dark gray)] to q_2 [red (light gray)], as defined in Fig. 1.

decay time for the center in our field configuration is found to be higher than estimated. We also leave open the question of pulse optimization utilizing methods such as gradient ascent pulse optimization (GRAPE) [16] or machine learning [55].

V. THE GERMANIUM-VACANCY CENTER

The germanium-vacancy center (GeV^-) has quite similar properties to the SiV^- center but exhibits stronger spin-orbit coupling, a larger discrepancy between the magnetic susceptibility of the ground and excited states, and longer excited-state lifetimes (narrower natural optical linewidths). As such it has the potential to be a superior qubit to SiV^-. In this section we therefore ask whether these discrepant properties might improve optical contrast—the primary limiting factor in the SiV^- measurements of Sec. III. Though we do not yet have as much information for this system, we can provide a rough estimate for the efficiency (fidelity) of a single-photon cavity-assisted measurement.

The GeV^- center forms the same split-vacancy structure as SiV^- and evolves under the same form of the Hamiltonian given in Eq. (1) [56]. In this case however the key ground-state parameters [56–63] are $g_S^{\perp} = 2.0023$, $\lambda^{(\mathrm{GS})} = 2\pi \times 181$ GHz, $g_S^{||,(\mathrm{GS})} = g_S^{\perp} - 0.006$, and $f^{(\mathrm{GS})} = 0.128$, while the corresponding excited-state parameters are $\lambda^{(\mathrm{ES})} = 2\pi \times 1120$ GHz, $g_S^{||,(\mathrm{ES})} = g_S^{\perp} - 0.1$, with $f^{(\mathrm{ES})} = 0.089$. Now for convenience here we have ignored the strain terms at present due to the already large energy separations, which should limit their impact. Further, phonon-induced decoherence for the GeV^- center should scale as either $e^{-8.7/T}$ or as T^3 [48], so that *absent new limiting factors*, reducing the temperature to 100 mK should improve the dephasing time from $T_2^* = 19$ ns [61] to at least 152 μs. The lifetimes of the optically excited states are 6 ns [56,62,64,65], and the branching ratios appear [61] consistent with those of the SiV^- center.

We are faced with significant uncertainty in estimating the low-temperature decay rates between the ground-state branches. Qualitatively, however, the system-environment coupling is likely much greater than for SiV^-: Despite much stronger spin-orbit coupling the experimentally determined coherence times for GeV^- are only $T_1 \geqslant 25$ μs and $T_2^* = 19$ ns at 2 K [61]. We may therefore expect that any population will relax quickly to the lower branch. We also note that for the expected two-photon relaxation process [48], the current T_1 and T_2^* times indicate a branching ratio to the lower branch on the order of 1000 : 1.

Our expectation of rapid ground-state decay motivates two significant modeling assumptions: First, the qubit *must* be encoded in the two lowest ground states (in contrast to SiV^-), restricting magnetic fields to $\leqslant 6.4$ T to prevent a crossing of the spin-orbit branches. Second, that decay from the upper ground states is faster than the time between measurement pulses, justifying their incorporation via a modification of optical branching ratios, rather than explicitly as states. Taking the extreme case of a 6.4 T magnetic field to maximize transition contrast, the ground-state frequencies are −191.65 GHz, 10.65 GHz, 12.28 GHz, and 168.72 GHz, while the excited-state frequencies are −657.04 GHz, −462.96 GHz, 478.91 GHz, and 641.09 GHz [see Fig. 4(a)].

In our measurement, using an optical transition between the GSM and ESM manifolds for state-dependent scattering, we target the transition between states of lowest energy (see Fig. 4). The nearest undesirable transition is −13.07 GHz detuned. This means that in conjunction with the narrow lifetime-limited linewidth of GeV^-, we expect that this center will tolerate larger cooperativities than SiV^- and so give higher measurement fidelities. This behavior is observed in Fig. 4, where a fidelity estimate above 0.999 is seen for cooperativities above 500 using a single-photon pulse (with a cooperativity of 50 we obtain comparable measurement fidelities to those for SiV^-). An increase in the measured T_2 time would, counterintuitively, require a greater cavity cooperativity (through changing branching ratios). Lowering the magnetic field to limit the phonon occupation number associated with ground-state transitions would reduce the optical transition contrast. Our estimates should therefore be interpreted in line with earlier SiV^- assumptions as outside projections of the center's potential.

Unlike the SiV^- case, single-qubit rotations performed using an optical STIRAP approach are not assessed for this system because the magnetic field required to identify the central excited states (∼40 T) is impractical. Instead one might drive a microwave transition between qubit levels (potentially with a strain field applied [27]).

VI. CONCLUSIONS

In this paper, three key observations have become apparent. First, cavity-mediated measurement should be possible on a timescale of order ∼20 ns with an error rate of order 1% for SiV (0.1% for GeV). Second, there is a trade-off in the field configuration between the lifetime of the qubit and the fidelity of STIRAP population transfer. Third, population transfer between encoded qubit states of SiV can, in principle, be achieved on a timescale of order ∼33 ns with a fidelity of order 97%. This estimated performance does not surpass that of the nitrogen-vacancy center [44,66].

Now despite operating in a field regime for which the coherence time is reduced, the potential of SiV^- for quantum information processing remains intact. Our single-qubit rotation, though limited to order 97%, remains competitive

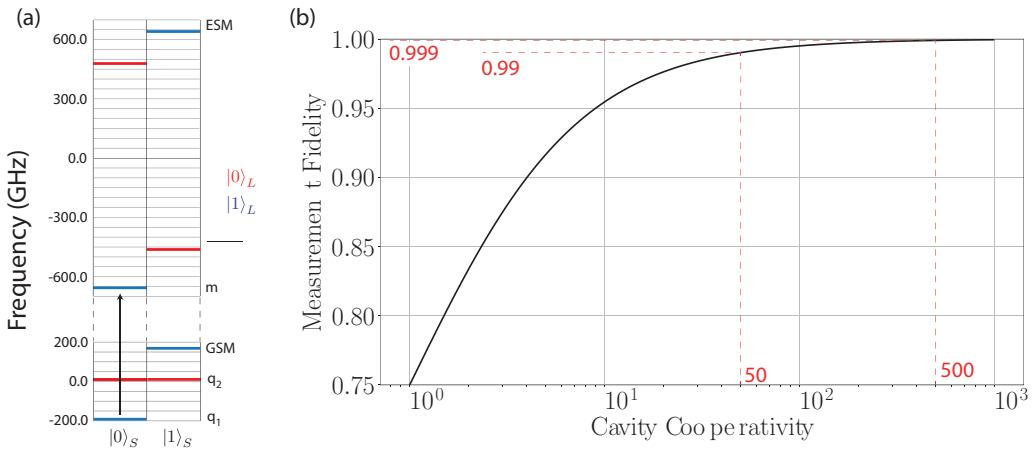

FIG. 4. (a) GeV^- energy level structure under a 6.4 T axial magnetic field. The target transition for measurement is denoted with a black arrow. (b) Estimated GeV^- measurement fidelity versus cooperativity, for one single-photon pulse and ideal source and detection efficiencies.

with prior experimental results [38] for optically mediated transfer. Prior results for direct transfer [27] reaching 99% observe measurement fidelities of order 90% and come at a cost to qubit lifetime similar to that which we observe. We do sacrifice long-time, high-fidelity single-qubit measurement and initialization [36,37] for shorter-time measurements with fidelities on the order of 99%. However, the approach we have taken is straightforwardly generalizable to two-qubit projective entanglement generation (formerly 95% [36]).

Distributed quantum information processing requires a more general set of operations than the use of SiV^- as a single-photon source. Correspondingly, there are drawbacks to focusing exclusively on performance derived from the long coherence times now available with the center. First, many photons weakly incident on the center reduce the fidelity of spin-photon entanglement generation. The small detuning between spin-selective optical transitions additionally limits the fidelity of small-photon-number adaptations through the T_2 time of the center. Second, in the presence of a nearby ^{29}Si nuclear spin, long-time operations will exceed the hyperfine period. They may therefore cause dephasing and reduce the fidelity of information stored in the nuclear spin state. Hyperfine parameters following transition to the excited states, so far unknown, exacerbate this issue. The coherence time was formerly the primary limiting factor for quantum information processing with SiV^-. Recent results [36,37] have shown that this is now only one in an array of important factors to be considered collectively. We hope that our results will encourage the exploration of more exotic field regimes, even where this may come at the cost of trading off performance in one area for another.

ACKNOWLEDGMENTS

We are very grateful to M. Trupke and A. Greentree for helpful comments. This project was made possible through the support of a grant from the John Templeton Foundation (JTF No. 60478). We also acknowledge support from the MEXT KAKENHI Grant-in-Aid for Scientific Research on Innovative Areas "Science of Hybrid Quantum Systems" (Grant No. 15H05870) and from the Japanese MEXT Quantum Leap Flagship Program (MEXT Q-LEAP), Grant No. JPMXS0118069605.

APPENDIX A: DETERMINING PARAMETERS

In this Appendix we discuss key assumptions and parameter regimes for the SiV^- beginning with strain.

1. Zero strain

When the strain terms are comparable to the spin-orbit splitting of the ground states, the orbital components of the two-qubit states are no longer orthogonal. In such a case a direct transition can be driven between the states of the spin component, though this comes at the expense of a direct relaxation process between the two-qubit states, decreasing the coherence time. This regime was investigated experimentally by Sukachev *et al.* [27] to achieve dynamical decoupling. A high-strain environment such as is explored in [48] might be used to manipulate optical transition detunings, in addition to raising the operating temperature.

For a strain tensor that does *not* mix axial with perpendicular components, the susceptibilities of the ground and excited states [48] were determined by Maity *et al.* [63]. For a discussion of the effects of strain on spin-photon interaction and transition contrast, see [29].

We have decided to leave these terms at zero. Strain terms strong enough to preserve the symmetry in transition overlap between the ground and excited states desired for the fast STIRAP pulses we are investigating would require a magnetic field two orders of magnitude larger than the current figure (9.179 T). Such strong fields are not believed to be experimentally feasible at the current time.

2. Optimistic assumptions

Not enough is yet known about the silicon-vacancy center to provide performance estimates at the level of precision required for scalable quantum information processing tasks. Here we deliberately take an optimistic view where we encounter uncertainty in the properties of the center, to clarify known limitations while leaving open the potential for

fortunate refinement in the future. Specifically, our assumptions are the following: no static Jahn-Teller terms (these are wrapped into strain); no fluctuation in the dynamical parameters; no nonradiative decay from the optically excited states; no native decay terms with decay times greater than $\sim 10\ \mu$s, which we justify by expected operation times; no nuclear (hyperfine) sublevels; and no additional energy levels around the optically excited states [25,67,68].

3. Ground-state decay times

For timescales of order tens of microseconds or below, the coherence time of the negatively charged silicon-vacancy center is dominated by thermal phonon interactions. Meesala *et al.* [48] identify three phonon-mediated spin decay processes: single-phonon transitions, two-phonon resonant transitions, and two-phonon off-resonance transitions. All three processes are caused by perturbative overlap in the spin projections of ground manifold energy eigenstates. Associated with the vanishing absorption components of these processes at low temperature or large fields are T_2 figures of order milliseconds and tens of milliseconds [27]. For population transfer, and also associated with inversion in the ground-state manifold caused by the large axial magnetic field of the second qubit regime in Sec. II, the emission rates of these phonon processes are also significant. Simply reducing the temperature is insufficient to suppress these emission rates.

Beginning with the zero-field regime, the orbital decay time from the upper branch is computed beginning with the 101 ns prefactor and about 45 GHz ground-state splitting for the rates of Jahnke *et al.* [50], relative to our chosen value of 51.5 GHz. Accounting for a cubic dependence on the energy gap, this provides a number of about 66 ns for direct orbital emission, from which we infer a conservative 6.6 μs figure for spin relaxation. As mentioned, this latter figure depends on perturbative spin-projection overlap; here it comes from the ratio between the observed T_1 (>1 s) and T_2 (13 ms) times of Sukachev *et al.* [27] (roughly 100 : 1), though we are aware that earlier figures could provide more optimistic ratios [25].

We move now to the second qubit regime with a magnetic field of $B_Z = 9.179$ T and $B_X = 0.600$ T. The single-phonon transition rate scales according to the overlap between an ideal initial state and its alternate-spin projection; our perpendicular magnetic field has been restricted to limit this overlap so that the alternate spin state is observed with probability less than 10^{-3}. Indeed, this restriction is a primary factor limiting the intensity of applied STIRAP pulses and the transition contrast in measurement mediated by a strongly coupled optical cavity. Under the assumption that perpendicular field perturbations can be expressed as some fraction 0.1%–0.01% of the dominant axial magnetic field, $B_Z = 9.179$ T, they contribute to order 0.01 T to 0.001 T. This is between 0.17% and 1.7% of the intentional 0.6 T perpendicular field, and should contribute correspondingly negligible spin-projection overlap. Remaining factors in the single-phonon transition rate are those governing standard absorption and emission: the thermal phonon occupation number, the phonon density of states, and the electron-phonon coupling. By assumption on the temperature, the first is low enough to make absorption rates negligible relative to the timescales of the operations we are considering (timescales of order 100 ns). The latter two we determine together by working backward again from the fit of Jahnke *et al.* [50], who obtain a prefactor of $1/(101 \times 10^{-9})$ Hz for an energy gap of order 50 GHz. For our magnetic field configuration, with a separation between qubit states of slightly less than 250 GHz, the cubic dependence of the combined density of states and electron-phonon coupling on the size of the energy gap yields an additional factor of roughly 125 ($250^3/50^3 = 5^3$). We therefore infer that the single-phonon transition rate should be approximately 1.25×10^5 Hz, giving a spin lifetime of order 8 μs under emission. This value, being only very approximate, is close enough to the 6.6 μs figure obtained from the zero-field regime that for simplicity we proceed with 6.6 μs for both regimes.

We note that the above estimates are extrapolated from figures measured in quite different field configurations from our own; if the spin decay time in particular is found to be longer than we predict, the performance of the operations we considered could be correspondingly improved.

APPENDIX B: CAVITY-MEDIATED REFLECTION CALCULATIONS

First we must expand the energy level structure of Eq. (1) to incorporate both ground and optically excited subspaces. This may be done by introducing an additional two-level system, and prefixing all Hamiltonian terms with a projector onto one or the other of the states of this system, which we will call the "transition" (TR) subsystem:

$$\hat{H}^{(\mathrm{GS})} \to \hat{H}^{(\mathrm{GS})} \otimes \hat{P}_0^{(\mathrm{TR})}, \quad \hat{H}^{(\mathrm{ES})} \to \hat{H}^{(\mathrm{ES})} \otimes \hat{P}_1^{(\mathrm{TR})}. \tag{B1}$$

The result leaves us with a new bare system Hamiltonian that is the tensor sum of the former individual cases:

$$\hat{H}_{\mathrm{sys}} = \hat{H}^{(\mathrm{GS})} \oplus \hat{H}^{(\mathrm{ES})}. \tag{B2}$$

Interactions between the SiV^- center and an optical cavity mode can now be expressed with a Jaynes-Cummings Hamiltonian in terms of combined operators of the optical-transition subsystem, the orbital angular momentum subsystem, and annihilation and creation operators of the harmonic mode,

$$\begin{aligned}\hat{H}_{\mathrm{int}} = \hbar g[&(\hat{c}_z^\dagger \hat{\sigma}_-^{(\mathrm{TR})} + \hat{c}_z \hat{\sigma}_+^{(\mathrm{TR})}) \\ &- \tfrac{1}{2}(\hat{c}_x^\dagger \hat{\sigma}_-^{(\mathrm{TR})} + \hat{c}_x \hat{\sigma}_+^{(\mathrm{TR})})\hat{\sigma}_x^{(o)} \\ &+ \tfrac{1}{2}(\hat{c}_y^\dagger \hat{\sigma}_-^{(\mathrm{TR})} + \hat{c}_y \hat{\sigma}_+^{(\mathrm{TR})})\hat{\sigma}_y^{(o)}],\end{aligned} \tag{B3}$$

where g is the vacuum-Rabi coupling, the factors of $1/2$ account for the difference in polarization coupling amplitudes, $\hat{\sigma}$ are the usual Pauli matrix operators, and we have further divided the harmonic mode into modes $\hat{c}_x$, $\hat{c}_y$, and $\hat{c}_z$, corresponding to different photon polarizations. This division allows us to define selection rules in the interaction Hamiltonian, corresponding to the configuration of spin and orbital angular momentum operators above.

The cavity modes now require their own self-energies,

$$\hat{H}_{\mathrm{cav}} = \hbar\omega_c(\hat{c}_z^\dagger \hat{c}_z + \hat{c}_x^\dagger \hat{c}_x + \hat{c}_y^\dagger \hat{c}_y), \tag{B4}$$

and the cavity must itself be coupled to external fields,

$$\hat{H}_{c-r} = \hbar\sqrt{\frac{\kappa_r}{2\pi}} \sum_{k\in\{x,y,z\}} \int_{\infty}^{\infty} d\omega(\hat{c}_k^{\dagger}\hat{r}_{k,\omega} + \hat{c}_k\hat{r}_{k,\omega}^{\dagger}),$$

$$\hat{H}_{c-t} = \hbar\sqrt{\frac{\kappa_t}{2\pi}} \sum_{k\in\{x,y,z\}} \int_{\infty}^{\infty} d\omega(\hat{c}_k^{\dagger}\hat{t}_{k,\omega} + \hat{c}_k\hat{t}_{k,\omega}^{\dagger}),$$

$$\hat{H}_{\text{fields}} = \hbar \sum_{k\in\{x,y,z\}} \int_{\infty}^{\infty} d\omega\, \omega(\hat{r}_{k,\omega}^{\dagger}\hat{r}_{k,\omega} + \hat{t}_{k,\omega}^{\dagger}\hat{t}_{k,\omega}), \tag{B5}$$

where k contains the polarization labels, ω is the angular frequency of the external field, $\hat{r}_{k,\omega}$ and $\hat{t}_{k,\omega}$ correspond to modes at the input and output mirrors of the cavity (r: reflection, t: transmission), and $\kappa_{r/t}$ denotes the rate of photon loss through each of these respective mirrors. Note that since the transmission port is not used for detection in this scheme, scattering from the cavity itself can be wrapped into the decay rate κ_t, so long as the ratio $\kappa_r : \kappa_t$ is adjusted appropriately.

We can now restrict ourselves to the single-excitation subspace and move to Fourier space to obtain a matrix Langevin equation set of the form

$$\left(\left[\begin{array}{ccc|c} \hat{H}^{(\text{GS})} & & & \hat{H}'_{\text{int},z} \\ & \hat{H}^{(\text{GS})} & & \hat{H}'_{\text{int},x} \\ & & \hat{H}^{(\text{GS})} & \hat{H}'_{\text{int},y} \\ \hline \hat{H}'^{\dagger}_{\text{int},z} & \hat{H}'^{\dagger}_{\text{int},x} & \hat{H}'^{\dagger}_{\text{int},y} & \hat{H}^{(\text{ES})} \end{array}\right] - \left[\begin{array}{c|c} i(\kappa_r+\kappa_t)\hat{I}_{12}/2 & \\ \hline & (\Delta_{\text{ac}} + i\gamma_{\text{opt}}/2)\hat{I}_4 \end{array}\right] - (\Delta_{\text{cf}} + E_{\text{GS}})\hat{I}_{16}\right)\bar{x} = -i\sqrt{\kappa_r}\left[\begin{array}{c} \bar{\delta}_{12} \\ \hline \bar{0}_4 \end{array}\right], \tag{B6}$$

where $\hat{I}_N$ is an $N \times N$ identity matrix, γ_{opt} is the optical decay rate of the center, Δ_{ac} is the frequency detuning between the target transition of the center and the cavity mode, Δ_{cf} is the frequency detuning between the cavity mode and the driving field, E_{GS} further shifts the frequency to align with the energy of the initial ground state, $\bar{\delta}_{12}$ is a 12×1 binary vector of Hamming weight 1 that determines the initial state and driving polarization, $\bar{0}_4$ is the 4×1 zero vector, and elements $\hat{H}'_{\text{int},k}$ (k the polarization as above) are single-photon components of the interaction matrix relating only to one of the three orthogonal photon polarizations, so that, e.g., the 8×8 submatrix

$$\left[\begin{array}{c|c} \hat{H}^{(\text{GS})} & \hat{H}'_{\text{int},y} \\ \hline \hat{H}'^{\dagger}_{\text{int},y} & \hat{H}^{(\text{ES})} \end{array}\right] \tag{B7}$$

corresponds to the restriction of $\hat{H}_{\text{sys}} + \hat{H}_{\text{int}}$ to consider only single, Y-polarized photons.

Using the now-standard input-output method of Collett and Gardiner [69], we find a series of equations of the form

$$r_{\text{out}}(t) = r_{\text{in}}(t) - i\sqrt{\kappa_r}c(t), \tag{B8}$$

for each of the states of the system (36 in total, most of which have a vacuum component for the input field). From this we obtain through the solution of the above matrix equation the scattering amplitudes of the cavity-center system.

Having determined the scattering amplitudes of the system, with the knowledge that we drive with only Z-polarized photons, and under the assumption that distinct scattering pathways dephase, we are then able to decompose an arbitrary density matrix into pure states, evolve each pure state according to these scattering amplitudes, and recollect the results. So long as the optical decay times are significantly faster that either the times between single-photon pulses or the ground-state decay times, the scattering process can be treated in secular fashion, and the approach repeated, projecting the state according to a selected branch of measurement outcomes.

We assume that the total decay rate of the cavity $\kappa_r + \kappa_t$ is equal to the optical decay rate of the center γ_{optical}, but the ratio between the rates for the individual mirrors is locally optimized via gradient descent, as are Δ_{ac} and Δ_{cf}.

1. Improved coherence times

In Sec. III we estimated a required spin decay time of 863 μs to achieve a measurement fidelity of 0.999. The parameters for which this time was obtained were the following: a cooperativity of 5, a trial (pulse) number of 31 (or similarly a weak coherent pulse with an average of one photon per 20 ns over a total time of 620 ns), an atom-center detuning of -94.500314 GHz, and a cavity-field detuning of -6.125525 GHz. For our field configuration, as the cooperativity is raised above 5, the performance is limited by a decreased transition contrast, while as it is lowered the increased contrast is outweighed by the increased measurement time.

2. Measurement pulse time

We have established minimum pulse times according to other decay terms. Assuming a Gaussian pulse for simplicity, a z score of -2.5 covers 0.49% of the pulse area, so that 99% of the pulse lies within a width of 5.16 standard deviations. We will call this the *width* of the pulse. The pulse time is limited by the lifetime of the center and the minimum energy gap between optical transitions. In our particular case, there exist two levels either side of the target that appear to interfere destructively; shown in Fig. 5 are example reflection (and complement) probabilities from the secondary (and target) qubit states. The target state achieves a maximum reflection probability of $O(99\%)$, the limiting fidelity of a single-shot, single-photon measurement. The error channel due to scattering is relatively insensitive to the bandwidth of the pulse.

With the aim of maximizing the reflection contrast between the two-qubit states, we therefore take $2\pi \times 0.71$ GHz as the rough upper bound on the total frequency width of the pulse,

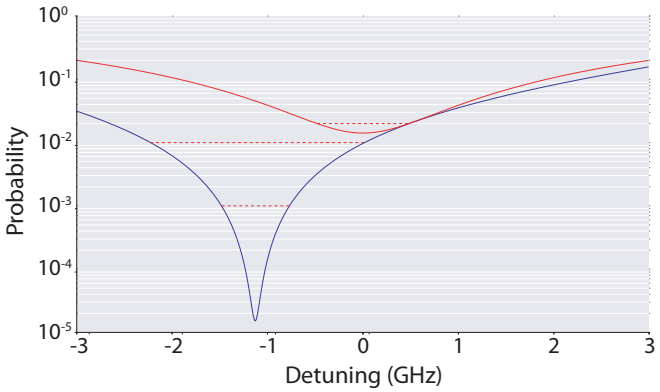

FIG. 5. The single-photon reflection probability for the secondary (blue, lower curve) qubit state and the complement (difference between 1 and this probability) for the target (red, upper curve) state, as functions of the frequency detuning between the cavity mode and the target transition of the SiV^- center. For this figure only, the incident field and cavity mode are resonant, the cavity mirrors are balanced, and the center-cavity cooperativity is 70. The peaks from the secondary qubit state appear to interfere destructively to suppress reflection close to the target transition. Units are expressed in pure frequencies. The red dashed lines are placed between the two curves at the levels 0.1%, 1%, and 2% as a guide to the eye emphasizing allowable pulse widths associated with these levels.

obtaining standard deviations in the frequency (σ_f) and time (σ_t) domains of

$$\sigma_f \leqslant \frac{2\pi \times 0.71\ \text{GHz}}{5.16} = 2\pi \times 0.13\ \text{GHz}, \tag{B9}$$

$$\sigma_t \geqslant \frac{1}{2\sigma_f} \geqslant 0.58\ \text{ns}. \tag{B10}$$

APPENDIX C: STIRAP MASTER EQUATION CALCULATIONS

For the STIRAP simulations of Sec. V we use a master equation of the standard Linblad form,

$$\frac{\partial}{\partial t}\hat{\rho} = \frac{-i}{\hbar}[\hat{H}_{\text{sys}} + \hat{H}_{\text{drive}}, \hat{\rho}] + \sum_{A,B\in S} \gamma_B^A L_B^A(\hat{\rho}), \tag{C1}$$

where S is the set of spin and angular momentum eigenstates, γ_B^A is the rate of decay from an initial state $|A\rangle$ to a final state $|B\rangle$, L_B^A is a Linblad superoperator based on this transition, i.e.,

$$L_B^A(\hat{\rho}) = |B\rangle\langle A|\hat{\rho}|A\rangle\langle B| - \frac{1}{2}(|A\rangle\langle A|\hat{\rho} + \hat{\rho}|A\rangle\langle A|), \tag{C2}$$

$\hat{H}_{\text{sys}}$ is the system Hamiltonian obtained by expanding Eq. (1) of the main text with an additional two-level system to allow for the optical degree of freedom (labeled "TR" for "transition," as described for the reflection calculations above), and $\hat{H}_{\text{drive}}$ is the driving Hamiltonian containing the STIRAP pulses,

$$\hat{H}_{\text{drive}}(t) = \frac{\hbar\Omega_{\max}}{\sqrt{2\pi}\sigma}\left[e^{\frac{-(t-\mu_+)^2}{2\sigma^2}} f_+(t)\hat{\sigma}_X^{(o)} + e^{\frac{-(t-\mu_-)^2}{2\sigma^2}} f_-(t)\right]\hat{\sigma}_X^{(\text{TR})}, \tag{C3}$$

$$f_\pm(t) = \cos(\omega_{(q_1,+)}t) \pm \cos(\omega_{(q_1,-)}t), \tag{C4}$$

where $\hat{\sigma}_X^{(o)}$ and $\hat{\sigma}_X^{(\text{TR})}$ are Pauli sigma-X matrix operators acting on the orbital and optical-transition degrees of freedom, respectively, $\Omega_{\max}$ is the maximum pulse amplitude expressed as an angular frequency, $t_{\max}$ is the total pulse time (from which the widths, $\sigma = t_{\max}/8$, and means, $\mu_\pm = (t_{\max} \pm \sigma)/2$, of the Gaussian window functions are determined), and $\omega_{(A,B)}$ is the angular frequency of the transition between states A and B, using the state labels of Fig. 1.

Enumerating states in S with the triplet labels XYZ, where $X, Y \in \{0, 1\}$ represent the orbital and spin degrees of freedom, respectively, and $Z \in \{G, E\}$ tracks whether the system is in the ground (G) or excited (E) states, the terms with nonzero rates of decay are set to

$$\begin{aligned}
\gamma_{00G}^{00E} = \gamma_{01G}^{01E} = \gamma_{10G}^{10E} = \gamma_{11G}^{11E} &= (4/6)/(2\pi \times 1.8\ \text{ns}),\\
\gamma_{10G}^{00E} = \gamma_{11G}^{01E} = \gamma_{00G}^{10E} = \gamma_{01G}^{11E} &= (2/6)/(2\pi \times 1.8\ \text{ns}),\\
\gamma_{00G}^{10G} = \gamma_{11G}^{01G} &= 1/(2\pi \times 66\ \text{ns}),\\
\gamma_{01G}^{00G} = \gamma_{11G}^{10G} &= 1/(2\pi \times 6.6\ \mu\text{s}),
\end{aligned} \tag{C5}$$

where the prefactors (4/6) and (2/6) account for the relative observed emission intensities of parallel and orthogonal photon polarizations [25,47], 1.8 ns is the optical decay time, and 66 ns (6.6 μs) is the orbital (spin) decay time in the ground-state manifold, as described in Appendix A 3.

[1] S. Wiesner, ACM Sigact News **15**, 78 (1983).
[2] P. W. Shor, in *35th Annual Symposium on Foundations of Computer Science, 1994 Proceedings* (IEEE Computer Society Press, Los Alamitos, CA, 1994), pp. 124–134.
[3] L. K. Grover, in *Proceedings of the 28th Annual ACM Symposium on Theory of Computing* (ACM, New York, 1996), pp. 212–219.
[4] D. Loss and D. P. DiVincenzo, Phys. Rev. A **57**, 120 (1998).
[5] B. E. Kane, Nature (London) **393**, 133 (1998).
[6] A. Zaitsev, *Optical Properties of Diamond: A Data Handbook* (Springer Science & Business Media, 2001).
[7] J. I. Cirac and P. Zoller, Phys. Rev. Lett. **74**, 4091 (1995).
[8] A. Blais, R.-S. Huang, A. Wallraff, S. M. Girvin, and R. J. Schoelkopf, Phys. Rev. A **69**, 062320 (2004).
[9] A. Wallraff, D. I. Schuster, A. Blais, L. Frunzio, R.-S. Huang, J. Majer, S. Kumar, S. M. Girvin, and R. J. Schoelkopf, Nature (London) **431**, 162 (2004).
[10] A. Steane, Rep. Prog. Phys. **61**, 117 (1998).
[11] J. Preskill, Quantum **2**, 79 (2018).
[12] H. J. Briegel, W. Dür, J. I. Cirac, and P. Zoller, Phys. Rev. Lett. **81**, 5932 (1998).
[13] N. Gisin, and R. Thew, Nat. Photonics **1**, 165 (2007).
[14] V. Giovannetti, S. Lloyd, and L. Maccone, Phys. Rev. Lett. **96**, 010401 (2006).

[15] V. Giovannetti, S. Lloyd, and L. Maccone, Nat. Photonics **5**, 222 (2011).

[16] N. Khaneja, T. Reiss, C. Kehlet, T. Schulte-Herbrüggen, and S. J. Glaser, J. Magn. Reson. **172**, 296 (2005).

[17] P. Král, I. Thanopulos, and M. Shapiro, Rev. Mod. Phys. **79**, 53 (2007).

[18] D. Dong and I. R. Petersen, IET Control Theory & Applications **4**, 2651 (2010).

[19] J. Li, X. Yang, X. Peng, and C.-P. Sun, Phys. Rev. Lett. **118**, 150503 (2017).

[20] D. A. Lidar, Adv. Chem. phys. **154**, 295 (2014).

[21] D. A. Lidar and T. A. Brun, *Quantum Error Correction* (Cambridge University Press, 2013).

[22] B. J. Brown, D. Loss, J. K. Pachos, C. N. Self, and J. R. Wootton, Rev. Mod. Phys. **88**, 045005 (2016).

[23] R. Harper and S. Flammia, Phys. Rev. Lett. **122**, 080504 (2019).

[24] F. Arute, K. Arya, R. Babbush, D. Bacon, J. C. Bardin, R. Barends, R. Biswas, S. Boixo, F. G. Brandao, D. A. Buell, and B. Burkett, Nature (London) **574**, 505 (2019).

[25] L. J. Rogers, K. D. Jahnke, M. H. Metsch, A. Sipahigil, J. M. Binder, T. Teraji, H. Sumiya, J. Isoya, M. D. Lukin, P. Hemmer *et al.*, Phys. Rev. Lett. **113**, 263602 (2014).

[26] G. Burkard, Physics **7**, 131 (2014).

[27] D. D. Sukachev, A. Sipahigil, C. T. Nguyen, M. K. Bhaskar, R. E. Evans, F. Jelezko, and M. D. Lukin, Phys. Rev. Lett. **119**, 223602 (2017).

[28] M. H. Metsch, K. Senkalla, B. Tratzmiller, J. Scheuer, M. Kern, J. Achard, A. Tallaire, M. B. Plenio, P. Siyushev, and F. Jelezko, Phys. Rev. Lett. **122**, 190503 (2019).

[29] C. T. Nguyen, D. D. Sukachev, M. K. Bhaskar, B. Machielse, D. S. Levonian, E. N. Knall, P. Stroganov, C. Chia, M. J. Burek, R. Riedinger, H. Park, M. Lončar, and M. D. Lukin, Phys. Rev. B **100**, 165428 (2019).

[30] F. Jelezko, I. Popa, A. Gruber, C. Tietz, J. Wrachtrup, A. Nizovtsev, and S. Kilin, Appl. Phys. Lett. **81**, 2160 (2002).

[31] C. Santori, P. Barclay, K. C. Fu, R. Beausoleil, S. Spillane, and M. Fisch, Nanotechnology **21**, 274008 (2010).

[32] R. Albrecht, A. Bommer, C. Pauly, F. Mücklich, A. W. Schell, P. Engel, T. Schröder, O. Benson, J. Reichel, and C. Becher, Appl. Phys. Lett. **105**, 073113 (2014).

[33] S. Johnson, P. Dolan, T. Grange, A. Trichet, G. Hornecker, Y.-C. Chen, L. Weng, G. Hughes, A. Watt, A. Auffèves *et al.*, New J. Phys. **17**, 122003 (2015).

[34] L. Robledo, H. Bernien, T. Van Der Sar, and R. Hanson, New J. Phys. **13**, 025013 (2011).

[35] J. Tetienne, L. Rondin, P. Spinicelli, M. Chipaux, T. Debuisschert, J. Roch, and V. Jacques, New J. Phys. **14**, 103033 (2012).

[36] M. K. Bhaskar, R. Riedinger, B. Machielse, D. S. Levonian, C. T. Nguyen, E. N. Knall, H. Park, D. Englund, M. Lončar, D. D. Sukachev, and M. D. Lukin, Nat. **580**, 60 (2020).

[37] J. N. Becker, B. Pingault, D. Groß, M. Gündoğan, N. Kukharchyk, M. Markham, A. Edmonds, M. Atatüre, P. Bushev, and C. Becher, Phys. Rev. Lett. **120**, 053603 (2018).

[38] J. N. Becker, J. Görlitz, C. Arend, M. Markham, and C. Becher, Nat. Commun. **7**, 13512 (2016).

[39] L.-M. Duan and H. J. Kimble, Phys. Rev. Lett. **92**, 127902 (2004).

[40] A. Young, C. Hu, L. Marseglia, J. Harrison, J. O'Brien, and J. Rarity, New J. Phys. **11**, 013007 (2009).

[41] K. Koshino and Y. Matsuzaki, Phys. Rev. A **86**, 020305(R) (2012).

[42] K. Nemoto, M. Trupke, S. J. Devitt, A. M. Stephens, B. Scharfenberger, K. Buczak, T. Nöbauer, M. S. Everitt, J. Schmiedmayer, and W. J. Munro, Phys. Rev. X **4**, 031022 (2014).

[43] S. Sun and E. Waks, Phys. Rev. A **94**, 012307 (2016).

[44] M. Hanks, M. Trupke, J. Schmiedmayer, W. J. Munro, and K. Nemoto, New J. Phys. **19**, 103002 (2017).

[45] K. Bergmann, N. V. Vitanov, and B. W. Shore, J. Chem. Phys. **142**, 170901 (2015).

[46] B. Pingault, J. N. Becker, C. H. H. Schulte, C. Arend, C. Hepp, T. Godde, A. I. Tartakovskii, M. Markham, C. Becher, and M. Atatüre, Phys. Rev. Lett. **113**, 263601 (2014).

[47] C. Hepp, T. Müller, V. Waselowski, J. N. Becker, B. Pingault, H. Sternschulte, D. Steinmüller-Nethl, A. Gali, J. R. Maze, M. Atatüre *et al.*, Phys. Rev. Lett. **112**, 036405 (2014).

[48] S. Meesala, Y.-I. Sohn, B. Pingault, L. Shao, H. A. Atikian, J. Holzgrafe, M. Gündoğan, C. Stavrakas, A. Sipahigil, C. Chia, R. Evans, M. J. Burek, M. Zhang, L. Wu, J. L. Pacheco, J. Abraham, E. Bielejec, M. D. Lukin, M. Atature, and M. Loncar, Phys. Rev. B **97**, 205444 (2018).

[49] J. L. Zhang, S. Sun, M. J. Burek, C. Dory, Y.-K. Tzeng, K. A. Fischer, Y. Kelaita, K. G. Lagoudakis, M. Radulaski, Z.-X. Shen *et al.*, Nano Lett. **18**, 1360 (2018).

[50] K. D. Jahnke, A. Sipahigil, J. M. Binder, M. W. Doherty, M. Metsch, L. J. Rogers, N. B. Manson, M. D. Lukin, and F. Jelezko, New J. Phys. **17**, 043011 (2015).

[51] B. Pingault, D.-D. Jarausch, C. Hepp, L. Klintberg, J. N. Becker, M. Markham, C. Becher, and M. Atatüre, Nat. Commun. **8**, 15579 (2017).

[52] Y.-I. Sohn, S. Meesala, B. Pingault, H. A. Atikian, J. Holzgrafe, M. Gündoğan, C. Stavrakas, M. J. Stanley, A. Sipahigil, J. Choi *et al.*, Nat. Commun. **9**, 2012 (2018).

[53] J. Wolters, A. W. Schell, G. Kewes, N. Nüsse, Schoengen, H. Döscher, T. Hannappel, B. Löchel, M. Barth, and O. Benson, Appl. Phys. Lett. **97**, 141108 (2010).

[54] A. D. Greentree, J. H. Cole, A. R. Hamilton, and L. C. L. Hollenberg, Phys. Rev. B **70**, 235317 (2004).

[55] P. B. Wigley, P. J. Everitt, A. van den Hengel, J. Bastian, M. A. Sooriyabandara, G. D. McDonald, K. S. Hardman, C. Quinlivan, P. Manju, C. C. Kuhn *et al.*, Sci. Rep. **6**, 25890 (2016).

[56] G. Thiering and A. Gali, Phys. Rev. X **8**, 021063 (2018).

[57] Y. N. Palyanov, I. N. Kupriyanov, Y. M. Borzdov, and N. V. Surovtsev, Sci. Rep. **5**, 14789 (2015).

[58] E. A. Ekimov, S. Lyapin, K. N. Boldyrev, M. V. Kondrin, R. Khmelnitskiy, V. A. Gavva, T. V. Kotereva, and M. N. Popova, JETP Lett. **102**, 701 (2015).

[59] V. Nadolinny, A. Komarovskikh, Y. Palyanov, I. Kupriyanov, Y. Borzdov, M. Rakhmanova, O. Yuryeva, and S. Veber, Phys. Status Solidi A **213**, 2623 (2016).

[60] E. A. Ekimov, V. S. Krivobok, S. G. Lyapin, P. S. Sherin, V. A. Gavva, and M. V. Kondrin, Phys. Rev. B **95**, 094113 (2017).

[61] P. Siyushev, M. H. Metsch, A. Ijaz, J. M. Binder, M. K. Bhaskar, D. D. Sukachev, A. Sipahigil, R. E. Evans, C. T. Nguyen, M. D. Lukin, P. R. Hemmer, Y. N. Palyanov, I. N. Kupriyanov, Y. M. Borzdov, L. J. Rogers, and F. Jelezko, Phys. Rev. B **96**, 081201(R) (2017).

[62] M. K. Bhaskar, D. D. Sukachev, A. Sipahigil, R. E. Evans, M. J. Burek, C. T. Nguyen, L. J. Rogers, P. Siyushev, M. H. Metsch, H. Park *et al.*, Phys. Rev. Lett. **118**, 223603 (2017).

[63] S. Maity, L. Shao, Y.-I. Sohn, S. Meesala, B. Machielse, E. Bielejec, M. Markham, and M. Lončar, Phys. Rev. Appl. **10**, 024050 (2018).

[64] T. Iwasaki, F. Ishibashi, Y. Miyamoto, S. Kobayashi, T. Miyazaki, K. Tahara, K. D. Jahnke, L. J. Rogers, B. Naydenov, F. Jelezko *et al.*, arXiv:1503.04938.

[65] K. Boldyrev, B. Mavrin, P. S. Sherin, and M. Popova, J. Lumin. **193**, 119 (2018).

[66] M. S. Everitt, S. Devitt, W. J. Munro, and K. Nemoto, Phys. Rev. A **89**, 052317 (2014).

[67] J. M. Higbie, J. D. Perreault, V. M. Acosta, C. Belthangady, P. Lebel, M. H. Kim, K. Nguyen, V. Demas, V. Bajaj, and C. Santori, Phys. Rev. Appl. **7**, 054010 (2017).

[68] S. Häußler, G. Thiering, A. Dietrich, N. Waasem, T. Teraji, J. Isoya, T. Iwasaki, M. Hatano, F. Jelezko, A. Gali *et al.*, New J. Phys. **19**, 063036 (2017).

[69] C. W. Gardiner and M. J. Collett, Phys. Rev. A **31**, 3761 (1985).